Flow Resistance of Metallic Screens in Liquid, Gaseous and Cryogenic Flow

Alexander Fischer and Jens Gerstmann
German Aerospace Center (DLR), Institute of Space Systems
Robert-Hooke-Straße 7, 28359 Bremen, Germany

Abstract

Fine metallic screens are important sub-systems in propellant tank systems of spacecrafts due to their application as filter devices. The flow resistance has to be known for a proper design of tank and feed line systems. In this paper the flow resistance of application-relevant metallic screens is investigated experimentally. The weave types "dutch twilled weave" (DTW) and "broad mesh" (BM) were studied. The description of BM geometry in literature is improper and a screen geometry model is developed, which is suitable for DTW and BM. The experimental data show good agreement with the literature.

1. Introduction

Woven fabrics are used in several technical applications. Filtering, screening, heat exchange or turbulence reduction, are just a few common examples. Several weave types are known from textile industry and provide a wide range of filter fineness depending on the individual weave type. In processes including chemical or mechanical restrictions or applications in high and very low temperatures metallic screens are used. One field of application is the filtration of propellant in the tank and feed line system of spacecrafts. A clean and pure supply of propellant is essential for proper engine performance and to prevent damage from the system. Additionally fine screens are used to prevent gas breakthrough up to a critical differential pressure and thus retaining gas bubbles in the liquid propellant flow. The exact knowledge of the filter screen characteristics, such as the flow resistance, is essential for the design of the propellant management system of spacecrafts. Pressure loss predictions in literature are not precise enough or not applicable to all types of weave. The available experimental data are not consistent for all screens. More experimental investigations are necessary together with a further development of the screen geometry model for other weave types.
This investigation focuses on the pressure loss at fine metallic screens, in particular dutch twilled and broad mesh screens. Major part of this study is the investigation of the BM 165x800 screen. The broad mesh weaves are slightly different compared to general dutch twilled weaves. They are woven more loosely and a gap exists between the shute wires. This has to be considered by comparing flow resistance behaviour of both weave types.

2. State of the art

2.1 Screen geometry

Due to the general application of fine screens in filtration, most previous investigations were done with stationary liquids or gases. However the application of fine metallic screens in spacecrafts, using liquid oxygen and hydrogen, extends the purpose of investigation with very low temperatures and liquids with low viscosity. In the literature only a few data exist for cryogenic liquids. Blatt[2] and Cady[3] investigated some screens with LH_2 and LN_2, but the actual progress in propellant management will lead to a new necessity for further data with cryogenic liquids.
In woven materials the arrangement of shute and warp wires leads to different kinds of weave types. They can be grouped in either weaves with an open area in the direction of flow (plain), or in tightly woven weaves (dutch). A woven screen is characterized by its type of weave and the count of warp and shute wires. The wire diameters can be different depending on the manufacturer. Tab. 1 shows the main characteristics of the most common weave types. Several investigations exist, relating to pressure loss on flow through metallic screens. Different descriptions for woven weaves with open pores treat the occurring pressure loss in analogy to an orifice, where the "open area" of a screen pore is the major influence in the description of the pressure loss[8][9][10][11]. Investigations concerning fine

weave types stated out, that the screen porosity and a pore diameter have major influence on the pressure loss[1][3][2][5][6]. They can be determined by experiment or taken from manufacturer specifications. Such descriptions are applicable for open weaves as well as for fine ones.
For computing porosity and pore diameter, a detailed model of the screen geometry is needed. Only a few investigations were done with regards to the weave geometry. Pedersen[8] and Rushton[12] investigated "open" weave types (like plain square or full twill weaves). Armour & Cannon[1] and Blass[4] investigated the closed woven dutch weaves. But none of the earlier investigations consider that there exists a special type of dutch twilled weave: the broad mesh weave. The difference between broad mesh and general dutch twilled weaves is the average distance between the shute wires (l_S). For dutch twilled weaves l_S nearly equals the shute wire diameter, the shute wires lie close to each other ($l_S \approx d_S$). For broad mesh weaves it is: $l_S \geq d_S$, only two shute wires lie close to each other, resulting in a gap between the pairs (see. Fig. 1). Due to the gap the screen porosity is significantly higher and the effective pore diameter greater compared with dutch twilled weaves.

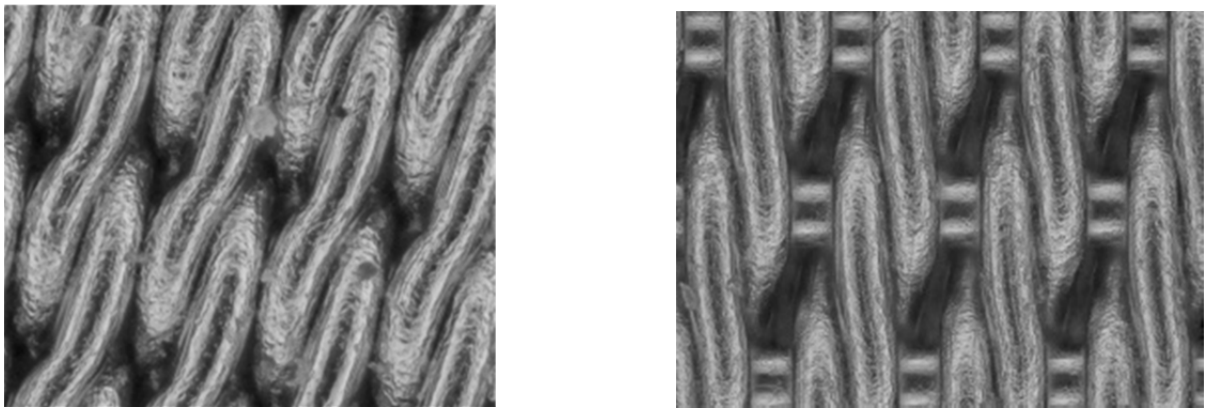

Figure 1: Comparison of DTW 200x1400 (left) and BM 165x800 (right) weave.
Wire diameters: d_S=40µm, d_K=70µm and d_S=52µm, d_K=70µm

Table 2: General overview of common weave types

Weave types with open gap		
Plain square	shute and warp wires passing over and under each other alternately $l_S = 1/n_S$, $l_W = 1/n_W$, $d_S \approx d_W$	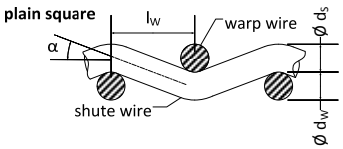
Full twill	shute and warp wires passing over and under two warp, respectively two shute wires, alternately $l_S = 1/n_S$, $l_W = 1/n_W$, $d_S \approx d_W$	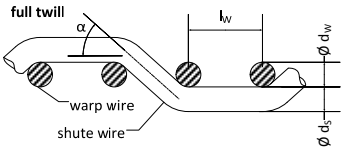
Semi twill	dependent on the type of semi twill the number of shute (warp) wires, passed under or over, is different $l_S = 1/n_S$, $l_W = 1/n_W$, $d_S \approx d_W$	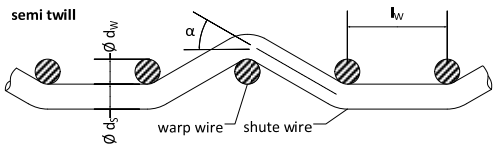
Fine weave types		

Plain dutch	shute wires passing under or over the warp wires alternately shute wires lie close to each other, no deformation $l_S = 1/n_S$, $l_W = 1/n_W$, $l_S \approx d_S$, $d_S < d_W$	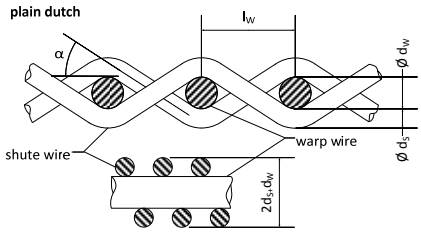
Dutch twilled	shute wires passing under and over the warp wires alternately shute wires are pressed close to each other, changing direction alternately under the angle γ $l_S = 2/n_S$, $l_W = 1/n_W$, $l_S \approx d_S$, $d_S < d_W$	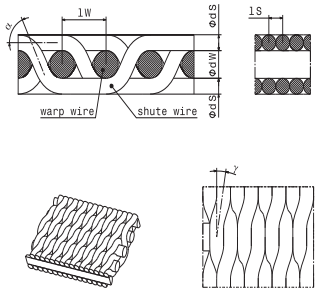
Broad mesh	likewise the dutch twilled shute wires lie not close to each other, but with space between <u>extremes:</u> no space: dutch twilled gap ≥ $2d_S$:straight shute wire lines $l_S = 2/n_S$, $l_W = 1/n_W$, $l_S \geq d_S$, $d_S < d_W$	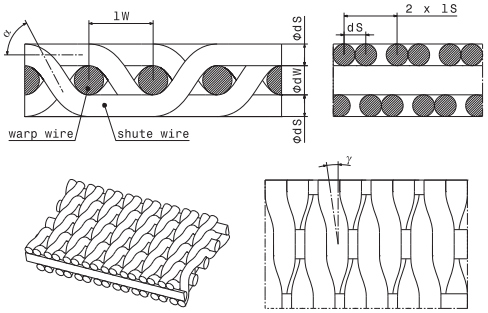

2.2 Screen resistance

The characteristic numbers determining the flow resistance are the Reynolds number (*Re*), prevailing the flow conditions, and the Euler number (*Eu*), which describes the occurring pressure loss in a fluid flow.

$$Eu = \frac{\Delta p}{\rho u^2}. \quad \textbf{(1)}$$

$$Re = \frac{\rho u D}{\mu} \quad \textbf{(2)}$$

With ρ the density, μ the viscosity, D the characteristic diameter, u the flow velocity and Δp the pressure drop.

In literature the pressure loss behaviour is commonly described with the dimensionless friction factor (*fr*). The friction factor is an extension of the *Eu* number with a ratio of geometrical screen properties. The definitions for *fr* and *Re* from several previous investigations are not consistent, because they are depending on different geometrical parameters (see Tab.1). The general form of correlating the friction factor with the *Re* number is given by:

$$fr = \frac{\alpha}{Re} + \beta. \quad \textbf{(3)}$$

Armour & Cannon[1] introduced a common formulation of *fr*, depending on fluid and screen properties. As geometrical parameter Armour & Cannon[1] used the effective pore diameter (D_P), the screen porosity (ε) and the surface area to unit volume ratio (a). Cady[3] and Blatt[2] used the same expression, but determined own coefficients and screen parameters. Ergun[5] and Belov[6] separately formulated a general formulation for predicting the pressure loss. The different definitions for *Re* and *fr* are listed together with the correlation coefficients in Tab. 1. Cady[3] and Erhardt[7] determined several other screen coefficients, in Tab. 1 the coefficients for the 165x800 and 200x1400 screen are listed exemplary. Within these predictions, the geometrical influence is tried to be considered with the effective pore diameter D_P of the screen (diameter of the biggest particles, which can pass through), the screen porosity ε (ratio of free fluid volume to total unit volume) and the surface area to unit volume ratio a (ratio between wire surface area and free fluid volume). However, no investigation considered the differing geometry of broad mesh compared to dutch twilled weaves. Most correlations were done with experimental determined values of the screen properties, or used manufacturer specifications. An exception is the formulation introduced by Erhardt[7]: he correlated his data without screen geometry influence, based only on flow properties, and determined coefficients for each screen and manufacturer separately. As a result the coefficients presented by Erhardt[7] are varying for different manufacturers of one screen and hence not applicable if another screen manufacturer is used. Tab. 1 gives an overview of the several considered pressure loss predictions. The correlations use a common relation of friction factor (*fr*) and Reynolds number (*Re*):

Table 1: pressure loss predictions

Armour & Cannon[1]	$\alpha = 8.61$	$\beta = 0.52$		
Cady 165x800[3]	$\alpha = 3.3$	$\beta = 0.17$	$fr_A = \frac{\Delta p}{\rho\frac{{u_0}^2}{\varepsilon^2}}\frac{D_P}{QB} = Eu\frac{\varepsilon^2 D_P}{QB}$	$Re_A = \frac{\rho u_0}{\mu a^2 D_P}$
Cady 200x1400[3]	$\alpha = 4.$	$\beta = 0.2$		
Blatt[2]	$\alpha = 2.49$	β=0.3		
Belov[6]	$\alpha = 72$	$\beta = 1.3$	$fr_{Be} = \frac{2\Delta p}{\rho\frac{{u_0}^2}{\varepsilon^2}}\frac{D_P}{QB} = Eu\frac{2\varepsilon^2 D_P}{QB}$	$Re_{Be} = \frac{\rho\frac{u_0}{\varepsilon}D_P}{\mu}$
Ergun[5]	$\alpha = 150(1\text{-}\varepsilon)$	$\beta = 1.75$	$fr_{Erg} = \frac{\Delta p}{\rho\frac{{u_0}^2}{\varepsilon^2}}\frac{\frac{6}{a}}{B}\frac{\varepsilon}{1-\varepsilon} = Eu\frac{6\varepsilon^3}{Ba(1-\varepsilon)}$	$Re_{Erg} = \frac{\rho u_0 \frac{6}{a}}{\mu}$
Erhardt* 165x800[7]	$\alpha = 22.9$	$\beta = 34.3$		
Erhardt* 200x1400[7]	$\alpha = 102$	$\beta = 183$	$fr_{Erh} = \frac{2\Delta p}{\rho {u_0}^2} = 2Eu$	$Re_{Erh} = \frac{\rho u_0 1 \mu m}{\mu}$

With Δp the occurring pressure loss and u_0 the average approaching fluid velocity, ρ the Density and μ the viscosity, and the screen characteristics: ε the porosity, D_P the effective pore diameter, Q the tortuosity factor (determined to be 1.3 for dutch twilled screens[1]), B the screen width and a the surface area to unit volume ratio.

The existing dimensionless correlations are not comparable directly in a common diagram, since the various correlations are based on different geometric screen factors. For a comparison the different correlations have to be converted into a common form. To enable a comparison the screen parameters pore diameter (D_P), screen porosity (ε) and surface area to unit volume ratio (a) of the BM 165x800 and the DTW 200x1400 screens are used to transfer the correlations into the expression given by Armour & Cannon[1]. They derived a general prediction for the pressure loss of the five common weave types. Their equations are applicable to calculate the influencing geometry parameters and to estimate the flow resistance. Only for dutch weave types the effective pore diameter is not provided and the information has to be determined by experiment or taken from manufacturers information. Fig. 2 shows the comparison of the considered prediction formulations (Blatt[2], Cady[3], Belov[6], Ergun[5] and Erhardt[7]) compared to literature data for the 165x800 and 200x1400 screens for example.

* Erhardt presented different coefficients for the single screen types each dependent on the screen manufacturer.

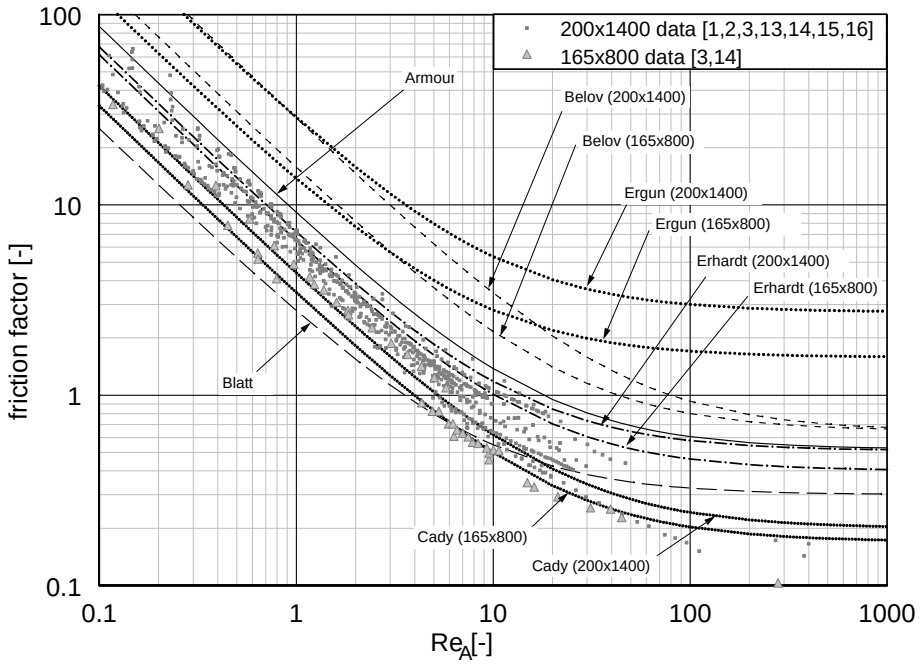

Figure 2: Friction factor in dependence on the Reynolds number, experiment data compared to theoretical predictions.

The predictions of Belov[6] and Ergun[5] show no agreement with the experimental data. Cady's[3] correlations fit well with the experimental data, but the coefficients are valid only for two dutch twilled and one broad mesh weave. Erhardt[7] defined a pressure loss prediction based on flow properties. He did not consider the screen and the coefficients determined for a single screen are varying for different manufacturers. The general correlation from Armour & Cannon[1] predicts higher friction factors than measured in the experiments[1,2,3,13,14,15,16]. Whereas the correlation of Blatt[2] predicts lower values for *fr*. Both correlations are based on data of five different weave types and do not predict the pressure loss for a single weave properly.

3 Screen model

The deviations between the measured pressure loss and the theoretical prediction are based on the problem to determine and to consider the real pore geometry. Formerly investigations have shown that the main geometry parameters are the screen porosity and the effective pore diameter, however both parameters have to be estimated and cannot be measured directly. In this study the geometry influence is considered using the screen porosity ε, which is defined as the ratio of void volume (V_{void}) and total volume (V_{total}), and a characteristic diameter D_{ch}, which is defined by the ratio of void volume and wire surface area (A_{wire}):

$$\varepsilon = \frac{V_{void}}{V_{total}} = \frac{V_{total} - V_{wire}}{V_{total}}, \tag{4}$$

$$D_{ch} = \frac{V_{void}}{A_{wire}} = \frac{V_{total} - V_{wire}}{A_{wire}}. \tag{5}$$

The characteristic diameter is defined as the reciprocal of Armour & Cannon's[1] ratio a. Wire volume and surface area are computable with four definite manufacturer properties: number of shute (n_S) and warp wires per inch (n_W) and the shute (d_S) and warp wire diameters (d_W). A weave is characterized by these properties and they do not vary between different manufacturers. No further information is needed or has to be determined. The sketch in Fig. 3 shows the geometrical model for dutch twilled and broad mesh weaves.

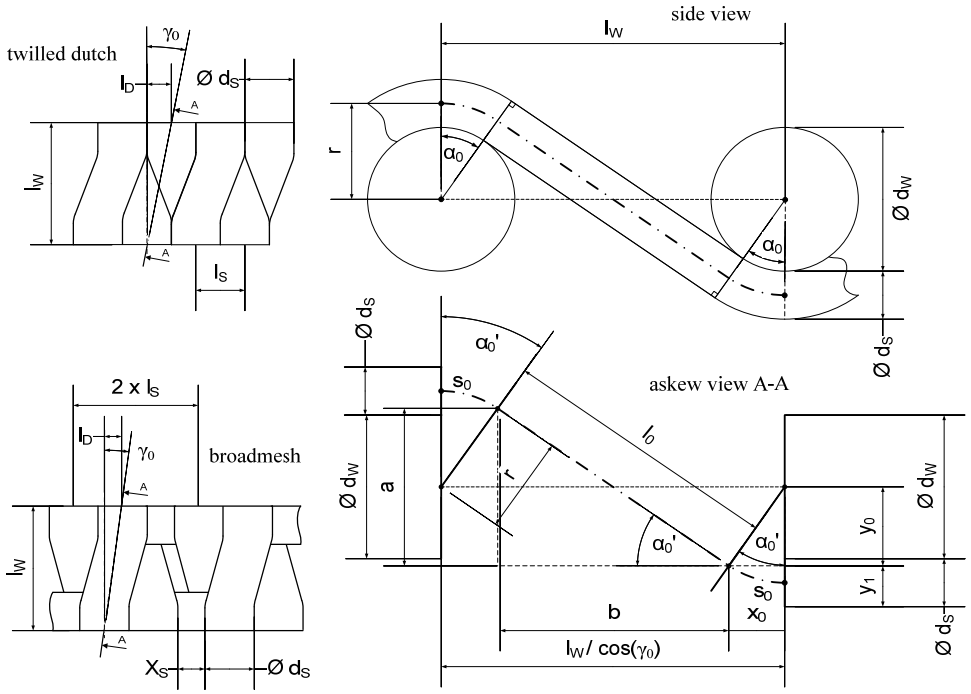

Figure 3: Sketch of the dutch twilled weave model. The broad mesh geometry differs in the spacing between the shute wires, where a gap occurs while the shute wires in dutch twilled weaves lie close to each other.

A description of the screen geometry is needed to calculate the wire volumes and surface areas of shute and warp wires. There is no deformation of the warp wires assumed, and they can be treated as straight cylinders. On the contrary the shute wires are deformed in two directions: they are passing over and under the warp wires alternately and changing direction through displacement due to the close packing of shute wires. A major influence is due to the deformation angle α_0. It is assumed that the askew angle nearly equals the straight angle: $\alpha`_0 \approx \alpha_0$. Following geometric values are defined:

Shute wire radius of curvature: $$r = \frac{d_S}{2} + \frac{d_W}{2}. \quad \textbf{(6)}$$

Average gap between shute wires: $$X_S = 2(l_S - d_S). \quad \textbf{(7)}$$

$X_S > 0$ for broad mesh weaves,
$X_S = 0$ is a typical dutch twilled weave

Note: Due to clinching of the shute wires the calculated values for X_S may be below zero, then X_S was assumed to be 0.

Length of displacement: $$l_D = \frac{-l_S}{4d_S} X_S + \frac{l_S}{2}. \quad \textbf{(8)}$$

$l_D = \frac{l_S}{2}$, for general dutch twilled.
$0 \leq l_D < \frac{l_S}{2}$, for broad mesh weaves.

Note: If $X_S \geq 2d_S$ it is $l_D = 0$, which means the shute wires are straight.

Displacement angle: $$\gamma_0 = \operatorname{atan}\left(\frac{l_D}{l_w}\right). \quad \textbf{(9)}$$

Auxiliary geometrical lengths:

$$x_0(\alpha_0) = r \times sin(\alpha_0), \quad \textbf{(10)}$$

$$y_0(\alpha_0) = r \times cos(\alpha_0), \quad \textbf{(11)}$$

$$y_1(\alpha_0) = \frac{d_w}{2} + d_S + y_0(\alpha_0), \quad \textbf{(12)}$$

$$a(\alpha_0) = d_K + 2d_S - 2y_1(\alpha_0), \quad \textbf{(13)}$$

$$b(\alpha_0) = \frac{l_w}{cos(\gamma_0)} - 2x_0(\alpha_0). \quad \textbf{(14)}$$

The equation which has to be solved to determine the deformation angle α_0 is given below. It is a non-linear equation and has to be solved numerically:

$$\tan(\alpha_0) = \frac{a(\alpha_0)}{b(\alpha_0)}. \quad \textbf{(15)}$$

Section lengths of the shute wire:

$$l_0(\alpha_0) = \sqrt{a(\alpha_0)^2 + b(\alpha_0)^2}, \quad \textbf{(16)}$$

$$s_0(\alpha_0) = r \times \alpha_0. \quad \textbf{(17)}$$

Total length of a shute wire:

$$L0_S = 2\frac{l_w}{cos(\gamma_0)} + 2(2s_0 + l_0). \quad \textbf{(18)}$$

Clinched shute wire diameter:

$$d_S = \sqrt{{d_{S0}}^2 \frac{4l_w}{L0_S}}. \quad \textbf{(19)}$$

d_{S0} = manufacturers diameter; $d_S < d_{S0}$.

The Eq.6- 19 have to be iterated several times until d_S converges, the starting value is: $d_S = d_{S0}$
It is now possible to calculate the unit volumes and surface areas of shute and warp wires:

Total unit volume:

$$V_{total} = 4l_w \times 2l_S \times (d_w + 2d_S). \quad \textbf{(20)}$$

Total wire volume:

$$V_{wire} = 4\left(\frac{\pi}{4}{d_S}^2 \times L0_S\right) + 4\left(\frac{\pi}{4}{d_w}^2 \times 2l_S\right). \quad \textbf{(21)}$$

Total wire surface area:

$$A_{wire} = 4(\pi d_S \times L0_S) + 4(\pi d_w \times 2l_S). \quad \textbf{(22)}$$

The screen properties ε and D_{ch} are defined in Eq. 4 and Eq. 5. The Reynolds number and the Euler number can now be calculated using these values:

$$Re_F = \frac{\rho\frac{u_0}{\varepsilon}D_{ch}}{\mu}, \quad \textbf{(23)}$$

$$Eu_F = \frac{\Delta p}{\rho\left(\frac{u_0}{\varepsilon}\right)^2}. \quad \textbf{(24)}$$

They are correlated directly to each other, similar to the correlations in the literature (Eq. 3):

$$Eu_F = \frac{A}{Re_F} + B. \quad \textbf{(25)}$$

With: ρ the Density, μ the viscosity, ε the porosity, Δp the occurring pressure loss and u_0 the average approaching fluid velocity. The fluid velocity within the screen is given by: $u_{screen} = u_0/\varepsilon$.

4. Experiment Setup

Two different test setups are designed to investigate the screen resistance. Different test fluids are used with different viscosity: water, GN_2 and LN_2. Thus it is possible to cover a broad *Re* range. One test setup is designed for experiments with water as test liquid. This setup is designed as a closed circuit with a controllable pump. The second experiment setup consists of a double cryostat configuration, enabling experiments with liquid Nitrogen (LN_2). Both cryostats are pressurized with gaseous Nitrogen to push the liquid through the test section. The pressurization part of this setup can be used for experiments with GN_2 as well.
The water setup allows continuous measurements and the experiments could be performed quickly. An adjustable rotary pump draws water from the storage tank which flow through a fine filter. The test section contains a 30mm diameter screen sample. The pressure difference across the screen is measured in the test section right before and after the sample. The volume flow is measured afterwards, before the water flows back into the storage tank. Additionally the pressure within the transfer line is measured for control issues. With the bypass line it is possible to keep the pump running, while the screen sample in the test section can be dismounted and changed.

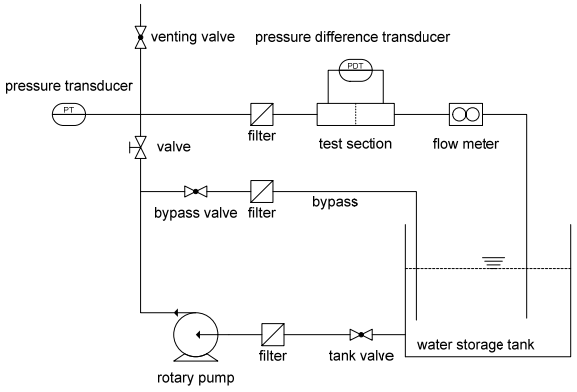

Figure 4: Sketch of the experiment setup for water tests.

For the LN_2 and GN_2 tests a section similar to the one for water is used. It contains a 15mm diameter screen sample. It is located, free ending, in the lower cryostat and is connected with the upper cryostat. The cryostats are chilled down and filled through the upper cryostat. The level of liquid nitrogen in each cryostat is determined continuously with capacitive level sensors. Both cryostats can be pressurised separately which allows measurements in both flow directions. The volume flow is determined by the continuous change of the fill level. The cryostats are pressurised with gaseous Nitrogen and the tank pressure is kept constant by an electrical pressure controller. To use this setup for experiments with gaseous Nitrogen, the test section can be connected directly with the gas supply section. The pressure difference is measured at the screen sample and the mass flow of the gas is measured with a thermodynamic sensor. The pressure controller allows the adjustment of the flow rates.

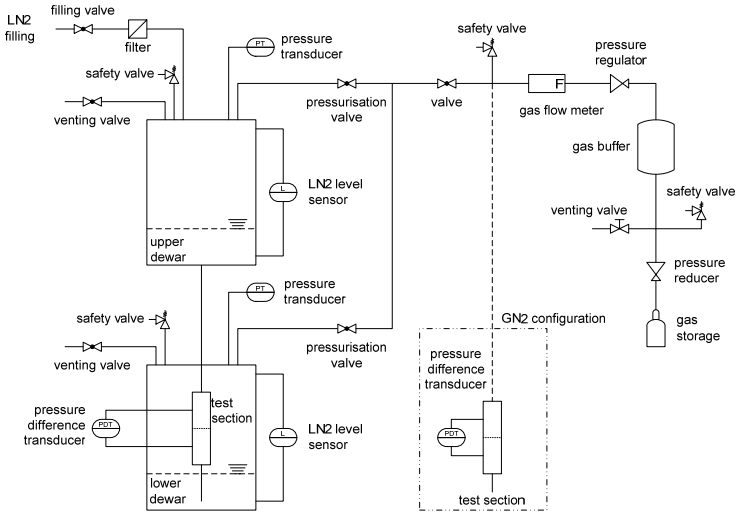

Figure 5: Sketch of the LN_2/GN_2 experiment setup.

5. Experiment Results

The pressure loss behaviour is depends on the occurring flow conditions, which can be described with the *Re* number. For low Re number ($Re_F < 5$) viscous forces are dominating the fluid flow, whereas for high Reynolds numbers ($50 < Re_F$) inertia forces are dominating. The transient region between laminar and turbulent flow lies in the range of $5 < Re_F < 50$. The respective region sizes and friction loss values are depending on the flow conditions and additionally on the individual screen characteristics (e.g. D_{ch}).
In Eq. 25 the first Term A/Re_F characterizes the laminar flow region. In double logarithmic expression the laminar region is characterized by a straight line with negative slope. The turbulent flow region characterized by the second term *B*, which is a constant and independent from the *Re* number. Considering Eq. 23 & 24 it means, that the pressure loss for laminar flow is proportional to the flow velocity *u* and for turbulent flow proportional to the square of the velocity u^2.

Table 3: Test parameters and fluid properties.

		GN_2[1]	LN_2	H_2O[2]
μ	[10^{-6} Pa*s]	17.66	163.8	760 – 993
ρ	[kg/m^3]	1.14 - 2.17	808.5	994.9 – 998.1
$\nu = \mu/\rho$	[10^{-6} m^2/s]	8.2 - 15.5	0.2	0.7 - 1.0
d_{Sample}	[mm]	15	15	30
u	[m/s]	1.19 – 14.6	0.11 – 1.33	0.14 – 0.71 (DTW) 0.14 – 0.85 (BM)
$\frac{\rho u d_{Sample}}{\mu}$	[-]	1,150 – 26,920	8,290 – 98,460	4,670 – 23,350 (DTW) 4,670 – 28,010 (BM)

1) the differing density is due to rising pressure with higher flow rates

2) the differing viscosity and density is due to different temperatures of the test fluid

To estimate the overall behaviour of the screen resistance (*Eu(Re)*) the complete flow regime has to be resolved. Experiments with fluids of different viscosity are necessary to carry out conditions from laminar to turbulent flow. The cryogenic test setup enables experiments with LN_2 to investigate the flow regime for high *Re* numbers. The laminar flow region is investigated performing experiments with GN_2. The water test setup is used for experiments in the transient region. In this study experiments were performed on the BM 165x800 screen with LN2, GN2 and water within a total range of $0.1 < Re_F < 150$. In addition four broad mesh and five dutch twilled screens were tested with water in a range of $1 < Re_F < 40$.
The measured experiment data are presented and discussed in the dimensionless form of Eu_F and Re_F given by Eq. 23 & 24. The necessary screen parameters D_{ch} and ε were computed and are listed in Tab. 4 together with the coefficients for each correlation of the investigated screens. The more loosely woven structure of the BM weaves is expressed by the values of ε and D_{ch}, which are in general higher compared to the DTW. Comparing the determined correlations it shows that the coefficients *B*, characterising the turbulent flow region, are significantly lower for BM compared to DTW.

Table 4: Screen properties and correlation coefficients.

weave	**mesh**	**d_S [µm]**	**d_W [µm]**	**ε**	**D_{ch} [µm]**	**A**	**B**
BM	165x800	52	70	0.448	10.67	43.13	2.70
	200x900	45	60	0.450	9.29	49.14	4.33
	200x600	45	60	0.582	16.35	44.77	3.01
	120x600	58	100	0.523	17.91	36.11	2.0
	120x400	58	100	0.623	28.57	39.26	2.4
DTW	325x2300	25	38	0.300	2.74	58.63	6.89
	200x1400	40	70	0.304	4.68	68.01	8.01
	165x1400	40	70	0.350	5.78	44.14	7.63
	80x700	76	100	0.391	12.30	48.96	7.61
	40x560	100	180	0.432	20.25	52.67	6.81

3.2 165x800 BM

With the BM 165x800 screen experiments were performed with water, gaseous and liquid Nitrogen. The experiment data are shown in Fig. 6. The GN_2 data cover the lower *Re* region ($0.1 < Re_F < 30$). The data in the higher *Re* region ($15 < Re_F < 150$) are determined with the LN_2 test liquid. Water experiments are carried out to resolve the transition region ($3 < Re_F < 60$). The allocation of the test fluids in different *Re* regions is due to their different kinetic viscosity (ν) (see Tab. 3). Decreasing of ν results in higher *Re* numbers. All measured data fit well into a single curve. The correlation was determined to be:

$$Eu_F = \frac{43.13}{Re_F} + 2.70 \tag{26}$$

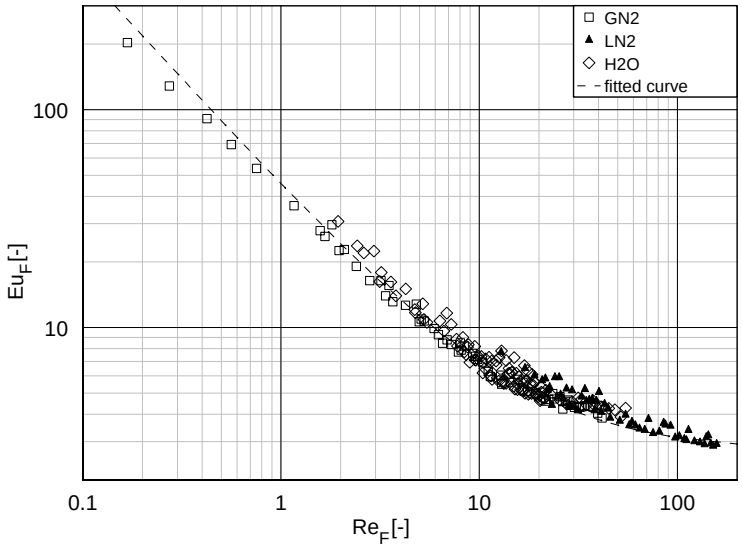

Figure 6: Present 165x800 experiment data.

Fig. 7 shows the experimental data of the present study compared with experimental data from Cady[3] and Sperling[14] as well as the correlations from Armour & Cannon[1], Cady[3] , Blatt[2] and Erhardt[7]. The experimental data show good agreement with data from Sperling[14] and Cady[3] in the low and transient *Re* region. For high *Re* numbers the data from Cady[3] is lower than the experimental data of this study.The proposed correlation (Eq. 26) shows a good agreement with the performed experimental data. The prediction of Armour & Cannon[1] generally results in higher values than the experimental data. The correlations of Blatt[2] and Erhardt[7] agree well with the performed experiments and with Sperling's[14] data. For the lower *Re* regime the correlation from Cady[3] agrees well with all experimental data. For higher *Re* regime Cady's[3] correlation predicts lower values for *Eu* than the measured data.

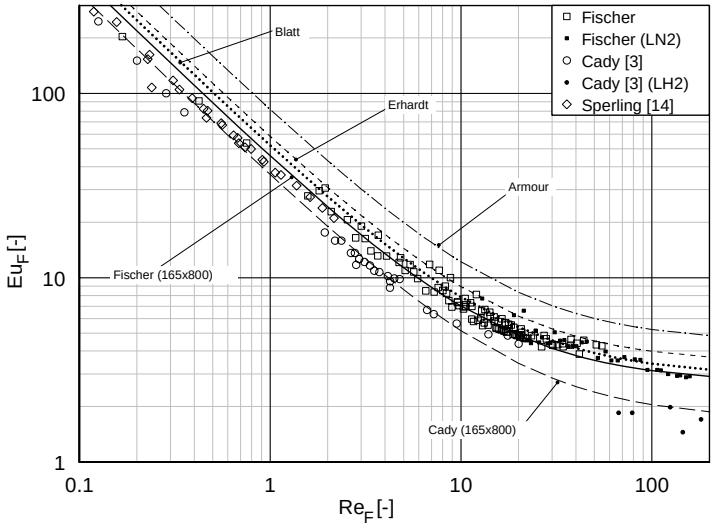

Figure 7: Eu_F vs. Re_F number for the BM 165x800 experimental data in comparison with pressure loss predictions.

3.2 200x1400 DTW

With the DTW 200x1400 screen experiments were performed with water. Fig. 8 shows the experimental data of the present study compared with experimental data from Armour & Cannon[1], Cady[3] , Blatt[2], Bruhn[13], Sperling[14], Stange[15] and Conrath[16] as well as the correlations from Armour & Cannon[1], Cady[3] , Blatt[2] and Erhardt[7]. The experimental data show good agreement with the literature data. The experiments with the 200x1400 screen were performed with water, covering a range of $1 < Re < 10$. The present correlation and the correlations proposed by Armour & Cannon[1], Cady[3] and Erhardt[7] agree well with the experimental data for the 200x1400 screen, where the correlation proposed by Blatt[2] does not agree. However for higher *Re* numbers the correlations predict different *Eu* numbers and the deviation of the experimental data is greater. Further research and experiments in this *Re* regime will be needed for a closer investigation.

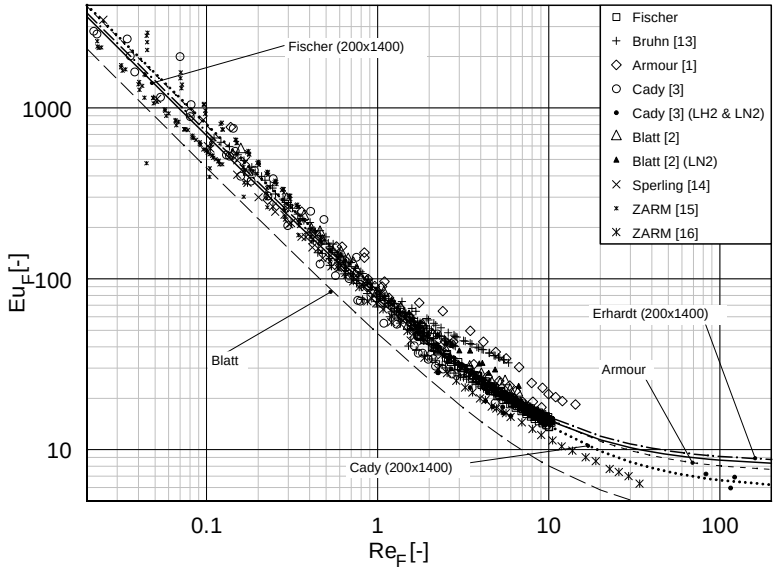

Figure 8: Eu_F vs. Re_F number for the DTW 200x1400 experimental data in comparison with pressure loss predictions.

5. Summary

Experimental results with respect to the flow resistance of different metallic screens are presented. A screen model is developed and the determined correlation is compared with experimental data and theory. The following metallic screens are investigated: dutch twilled weave (DTW): 325x2300, 200x1400, 165x1400, 80x700, 40x560 and broad mesh (BM): 165x800, 200x900, 200x600, 120x600, 120x400. The test fluids are water, as well as liquid and gaseous Nitrogen.

For dimensionless presentation using the Euler and the Reynolds number a correlation is developed, considering the geometrical differences between dutch twilled and broad mesh weaves. Used parameters in the model are the screen porosity ε and the characteristic screen diameter D_{ch}, both parameters mainly influence the pressure loss at woven weaves and can be calculated with the knowledge of four available manufacturer specifications: the shute and warp wire counts and their corresponding wire diameters. Thus a single weave type is characterized distinctly. No further experimental determined properties, e.g. the effective pore diameter, are necessary. The geometrical screen properties are calculated for the investigated screens. A dimensionless presentation is proposed applying the *Eu* number and *Re* number, which is applicable for DTW weaves and agrees with existing pressure loss predictions for this weave type. The proposed correlation extends the applicability for BM screens, where the prediction of Armour & Cannon[1] is not applicable properly. The predictions of Cady[3], and Erhardt[7] were found to be applicable at least in lower and transient *Re* region. The prediction of Blatt[2] is found to be applicable only for the 165x800 screen. The experimental data agrees well with the data from literature. For the high *Re* regime more experimental data are needed to validate the screen resistance models.

References

[1] J.C.Armour, J.N. Cannon. 1968. Fluid Flow Through Woven Screens. In *AIChE J. 14 (3)*. 415-420

[2] M.H.Blatt et. al. Nov. 1970. Low Gravity Propellant Control Using Capillary Devices in Large Scale Cryogenic Vehicles- Related Irad Studies. *General Dynamics/Convair (NASA CR-102902)*

[3] E.C.Cady. Aug. 1973. Study of Thermodynamic Vent and Screen Baffle Integration for Orbital Storage and Transfer of Liquid Hydrogen. *MDAC Rept. MDC G4798*.

[4] E. Blass. 1964. Geometrische und Strömungstechnische Untersuchungen. *Chemie-Ing.-Techn. 36. Nr 7*

[5] S.Ergun. 1952. Fluid Flow Through Packed Columns. *Chem. Eng. Prog. 48.* 89-94

[6] S.V.Belov. 1990. Hydraulic Resistance of Woven Metal Screens. *New Machinery and Equipment*

[7] G.Erhardt. 1983. Flow measurement on wire gauzes. *Int. Chem. Eng. No. 3*. 455-464

[8] G.C.Pedersen. 1969. Fluid Flow through Monofilament fabrics. *Paper presented at 64th National Meeting of AIChE*

[9] W.M. Lu et. al. 1996. Fluid Flow through basic weaves of monofilament filter cloth. *Textile Research Journal 66 (5)*, 311-323

[10] S.F.Hoerner. 1952. Aerodynamic Properties of Screens and Fabrics. *Textile Research Journal Vol. 22, No. 4.* 274-280.

[11] J.W. Park et. al. 2001. Thermal/fluid Characteristics of Isotopic Plain-weave Screen Laminates as Heat Exchange Surfaces. *AIAA 2002-0208*.

[12] A.Rushton and P. Griffiths. 1971. Fluid Flow in Monofilament Filter Media. *Trans. Inst. Chem. Eng. 49*. 49-59

[13] H. Bruhn. 1985. Siebwiderstandsmessungen mit Sieben der Maschenweite 9-10µm und 12-14µm unter Verwendung von Flüssigkeiten mit unterschiedlicher Zähigkeit, *FFE- Tanktechnologie, MBB-ERNO-Mitteilungen*

[14] O. Sperling. 1996. Experimentelle Bestimmung des Siebwiderstandes von Filtern in einer Fluidströmung. *Studienarbeit, Uni Bremen, ZARM*

[15] M. Stange and M. Michaelis. 1998. Untersuchung des Siebwiderstandes eines WINTEC Testsiebes. *Bericht ZARM*.

[16] M.Conrath and M. Dreyer. 2010. Gas separation and bubble behavior at a woven screen. *J. Mult. Flow*.

[17] M. Ludewig, et. al. 1974. Pressure Drop Across Woven Screens under Uniform and Nonuniform Flow Conditions. *Final Report NAS8-28736*